Egypt. J. Chem. **Vol. 68,** SI: Z. M. Nofal, pp. 789 - 802 (2025)

Egyptian Journal of Chemistry

http://ejchem.journals.ekb.eg/

A Novel Series of Benzimidazole-Triazole-Tetrazole Compounds: Synthesis, Structural Analysis, and Cytotoxic Activity against MCF-7 Cells

Adel H. Abdel-Rahman [1], Magdi E. A. Zaki [2], Ibrahim F. Zaid [1], Wafaa M. Salama [1], Mohamed A. Hawatah [1], Yasser H. Zaki [3]*, Sobhi M. Gomha [4]*, Basant Farag [5], Fathy E. Abdelgawad [4], and Hamada H. Amer [6,7]

[1] *Department of Chemistry, Faculty of Science, Menoufia University, Shebin El-Koam, 3251, Egypt*
[2] *Department of Chemistry, Faculty of Science, Imam Mohammad Ibn Saud Islamic University (IMSIU), Riyadh 11623, Saudi Arabia*
[3] *Department of Chemistry, Faculty of Science, Beni-Suef University, Beni-Suef, 62514, Egypt*
[4] *Department of Chemistry, Faculty of Science, Islamic University of Madinah, Madinah 42351, Saudi Arabia*
[5] *Department of Chemistry, Faculty of Science, Zagazig University, 44519 Egypt*
[6] *Animal Medicine and Infectious Diseases Department, Faculty of Veterinary Medicine, University of Sadat City, 2958, Egypt*
[7] *Chemistry Department, University College of Turabah, Taif University, Turabah, Taif, 21944, Saudi Arabia*

Abstract

A novel series of benzimidazolo-[1,2,4]triazole-tetrazole derivatives was synthesized and evaluated for anticancer potential through integrated in silico and in vitro approaches. Molecular docking against the 8GVZ anticancer target revealed that compounds **4, 5, 7, 9,** and **11** exhibited superior binding affinities, surpassing the reference drug 5-fluorouracil. ADMET predictions confirmed favorable pharmacokinetic and toxicity profiles, supporting their drug-likeness. Subsequent in vitro assays against MCF-7 breast cancer cells demonstrated potent cytotoxicity, with compound **11** showing the lowest IC_{50} value (0.21 µM). These findings highlight compound **11** and its analogs as promising leads for further anticancer drug development.

Keywords: Benzimidazoles, Triazoles, Tetrazoles, Anticancer, Computational Modeling, ADMET Prediction

1. Introduction

Heterocyclic compounds such as benzimidazoles, triazoles, and tetrazoles play a vital role in medicinal chemistry due to their broad-spectrum biological activities. Benzimidazoles, in particular, have demonstrated significant antimicrobial, antiviral, anti-inflammatory, and antitumor properties, making them key scaffolds in anticancer drug development owing to their structural versatility and synthetic accessibility [1–10]. Notable examples include bendamustine, carbendazim, and veliparib, as well as Topo I inhibitors like Hoechst derivatives [11–14].

Triazoles are a versatile class of heterocycles extensively studied for their wide-ranging biological activities. They exhibit potent antimicrobial, antifungal, antiviral, anti-inflammatory, and anticancer properties, making them valuable cores in drug design [15-22]. Triazoles, valued for similar bioactivities, are often combined with benzimidazole frameworks to enhance therapeutic potential, with recent studies highlighting their notable anticancer efficacy and Topo II inhibition [23–27]. Tetrazoles, also widely utilized, contribute additional pharmacological benefits and are frequently incorporated into hybrid molecules targeting cancer and infectious diseases [28–39].

Due to the cost and limitations of experimental screening, in silico methods have become crucial for early prediction of pharmacokinetic and safety profiles in drug development. Computational tools, particularly molecular docking, are widely used to assess interactions between novel compounds and target proteins. In this study, docking simulations evaluated the binding of synthesized benzimidazolo-triazole-tetrazole derivatives (compounds 1–11) with an anticancer target protein (PDB ID: 8GVZ). PyMOL was employed for 3D visualization of protein-ligand interactions [40]. Compounds showing the strongest binding affinities were further evaluated using the MTT assay on MCF-7 breast cancer cells, with 5-fluorouracil (5-FU) as a standard reference [41]. ADMET profiling—covering absorption, distribution, metabolism, excretion, and toxicity—was also performed to assess the pharmacokinetic properties essential for drug safety and efficacy [42–44].

*Corresponding author e-mail: Yasser.Hassan@science.bsu.edu.eg (Y.Z.); smgomha@iu.edu.sa (S.G.)
Received date 12 March 2025; Revised date 25 April 2025; Accepted date 10 June 2025
DOI: 10.21608/ejchem.2025.367652.11440

Building on our continued efforts to develop biologically active compounds [45–57], we designed, synthesized, and evaluated a new series of benzimidazolo-triazole-tetrazole derivatives for anticancer potential. This work included structural characterization, in silico molecular docking to predict target protein interactions, and ADMET profiling to assess pharmacokinetic properties. The most promising compounds were further tested against MCF-7 breast cancer cells to identify potential therapeutic leads.

2. Experimental

2.1 Chemistry

Melting points were determined using a Kofler block apparatus and are uncorrected. IR spectra were recorded on a Perkin-Elmer 1720 FTIR spectrometer (cm^{-1}) using KBr disks. ^{1}H NMR spectra were measured on a Varian Gemini spectrometer (300 MHz) using DMSO-d_6 as the solvent and TMS (δ) as the internal standard. Mass spectra were obtained using a Shimadzu Gas Chromatography Mass Spectrometer (GC-MS) model GC 2010 (70 eV). The progress of reactions was monitored by thin-layer chromatography (TLC) using aluminum silica gel plates 60 F_{245}. The anticancer activity of the synthesized compounds was evaluated at the National Cancer Institute (NCI) in Cairo, Egypt. Additionally, anticancer activity against breast cancer was tested at El-Azhar University.

Synthesis of 3-(5-(2-(3-methyl-*1H*-benzo[4,5]imidazo[2,1-*c*][1,2,4]triazol-1-yl)ethyl)-*2H*-tetrazol-2-yl)propanenitrile (2)

A solution of 1-(2-(2H-tetrazol-5-yl)ethyl)-3-methyl-1H-benzo[4,5]imidazo[2,1-c][1,2,4]triazole **(1)** (2.68 g, 10 mmol) in N,N-dimethylformamide (10 mL) was heated to reflux at 180°C for 30 minutes to 1 hour. The mixture was then cooled to room temperature, followed by the addition of malononitrile (0.52 g, 10 mmol). The reaction was refluxed for an additional 6 hours, after which the precipitate was collected by filtration using ethanol, and recrystallized from DMF, yielding pale yellow crystals. Yield: 1.01 g (60%); m.p. > 300°C. IR (KBr): *ν* cm^{-1} ν_{max}: 3058 (CH aromatic), 2927 (CH aliphatic), 2373 (CN), ^{1}H NMR (300 MHz, DMSO-d_6) *δ*: 2.12 (3H, s, CH_3), 3.00 (2H, t, *J* = 5.00 Hz, CH_2), 4.05 (2H, t, *J* = 4.50 Hz, CH_2), 3.20 (2H, t, *J* = 5.5 Hz, CH_2), 4.12 (2H, t, *J* = 4.2 Hz, CH_2), 6.95-7.85 (4H, m, Ar-H) ppm; ^{13}C NMR (100 MHz, DMSO–d_6) δ: 14.8, (CH_3), 15.3, 29.8, 59.6, 62.9, 113.4, 119.7, 121,3, 125.1, 137.4, 142.1, 144.7, 150.8, 166.5 ppm; EI-MS: *m/z* = 321 [M^+]. Anal. Calc. for $C_{15}H_{15}N_9$: C, C, 56.07; H, 4.71; N, 39.23. Found C, 56.19; H, 4.84; N, 39.37%.

Synthesis of 1-(2-(2-(2-(*2H*-tetrazol-5-yl)ethyl)-*2H*-tetrazol-5-yl)ethyl)-3-methyl-*1H*-benzo[4,5]imidazo[2,1-*c*][1,2,4]triazole (3)

Nitrile derivative **2** (3.21 g, 10 mmol), sodium azide (0.7 g, 10 mmol), and ammonium chloride (0.6 g, 10 mmol) were heated in N,N-dimethylformamide (10 mL) at 140°C for 3 hours. After the reaction, the solvent was removed under reduced pressure, and the residue was dissolved in 10 mL of water. Acidification of this solution to pH 2 with concentrated hydrochloric acid in an ice bath caused the precipitation of the tetrazole, which was then filtered, dried, and recrystallized from DMF, to obtain compound **3** as pale yellow crystals (63%), m.p. > 300°C. IR (KBr) cm^{-1} ν_{max}: 3426 (NH), 2911 (CH), 1626 (C=N), 1085 (N=N); ^{1}H NMR (300 MHz, DMSO-d_6): *δ* =1.95 (3H, s, CH_3), 3.00 (4H, t, *J* = 5.5 Hz, $2CH_2$), 4.04 (4H, t, *J* = 4.2 Hz, $2CH_2$), 6.93-7.85 (4H, m, Ar-H), 9.10 (1H, brs, NH) ppm; EI-MS: m/z = 364 [M^+]. Anal. Calc. for $C_{15}H_{16}N_{12}$: C, 49.44; H, 4.43; N, 46.13. Found C, 49.57; H, 4.60; N, 46.25%.

Synthesis of ethyl 2-(5-(2-(5-(2-(3-methyl-*1H*-benzo[4,5]imidazo[2,1-*c*][1,2,4]triazol-1-yl)ethyl)-*2H*-tetrazol-2-yl)ethyl)-*2H*-tetrazol-2-yl)acetate (4)

Dissolving compound **3** (3.64 g, 10 mmol) in dry dimethylformamide (10 mL), anhydrous potassium carbonate (1.38 g, 10 mmol) and ethyl chloroacetate (1.22 g, 10 mmol) were added. This mixture was stirred at room temperature for 6 hours. The resulting precipitate was poured onto crushed ice, filtered, and dried, and recrystallized from EtOH, affording a brown powder (56%), m.p. 295-297°C. IR (KBr) cm^{-1} ν_{max}: 2982 (CH), 1737 (C=O); ^{1}H NMR (300 MHz, DMSO-d_6): *δ* =1.24 (3H, t, *J* = 7.2 Hz, $CH_2\underline{CH_3}$), 1.95 (3H, s, CH_3), 3.00 (4H, t, *J* = 5.5 Hz, $2CH_2$), 4.04 (4H, t, *J* = 4.2 Hz, $2CH_2$), 4.15 (2H, q, *J* = 5.5 Hz, $\underline{CH_2}CH_3$), 4.55 (2H, s, CH_2), 6.75-7.82 (4H, m, Ar-H) ppm; EI-MS: *m/z* = 450 [M^+]. Anal. Calc. for $C_{19}H_{22}N_{12}O_2$: C, 50.66; H, 4.92; N, 37.31. Found C, 50.78; H, 4.79; N, 37.43%.

Synthesis of 2-(5-(2-(5-(2-(3-methyl-*1H*-benzo[4,5]imidazo[2,1-*c*][1,2,4]triazol-1-yl)ethyl)-*2H*-tetrazol-2-yl)ethyl)-*2H*-tetrazol-2-yl)acetohydrazide (5)

A mixture of compound **4** (4.50 g, 10 mmol) and hydrazine hydrate (10 mL) was heated under reflux for 4 hours. After concentration and cooling, the mixture was poured over crushed ice. The resulting precipitate was filtered and dried, dried, and recrystallized from DMF, affording a brownish powder (63%), m.p. > 300°C. IR (KBr) cm^{-1} ν_{max}: 3422, 3450 (NH_2), 3334 (NH), 2928 (CH), 1687 (C=O); ^{1}H NMR (300 MHz, DMSO-d_6): *δ* =1.95 (3H, s, CH_3), 2.43 (2H, brs, NH_2), 3.00 (4H, t, *J* = 5.5 Hz, $2CH_2$), 4.04 (4H, t, *J* = 4.2 Hz, $2CH_2$), 4.55 (2H, s, CH_2), 6.75-7.82 (4H, m, Ar-H), 8.56 (1H, brs, NH) ppm; EI-MS: *m/z* = 436 [M^+]. Anal. Calc. for $C_{17}H_{20}N_{14}O$: C, 46.78; H, 4.62; N, 44.93. Found C, 46.64; H, 4.50; N, 45.05%.

Synthesis of 1-(2-(2-(2-ethoxyethyl)-*2H*-tetrazol-5-yl)ethyl)-3-methyl-*1H*-benzo[4,5]imidazo [2,1-*c*][1,2,4]triazole (6)

Compound **1** (2.68 g, 10 mmol) and 1-bromo-2-ethoxyethane (1.52 g, 10 mmol) were dissolved in N,N-dimethylformamide (10 mL), and the mixture was refluxed for 6 hours. After concentrating and cooling, the reaction mixture was poured onto crushed ice. The resulting precipitate was filtered, dried, and recrystallized from DMF, affording a yellow powder (81%), m.p. > 300 °C. IR (KBr) cm^{-1} ν_{max}: 2931 (CH), 1387 (C-O), ^{1}H NMR (300 MHz, DMSO-d_6): *δ* =1.12 (3H, t, *J* = 7.2 Hz, $CH_2\underline{CH_3}$), 1.95 (3H, s, CH_3), 3.00 (4H, t, *J* = 5.5 Hz, $2CH_2$), 4.04 (4H, t, *J* = 4.2 Hz, $2CH_2$), 3.85 (2H, q, *J* = 5.5 Hz, $\underline{CH_2}CH_3$), 7.22-8.24 (4H, m, Ar-H) ppm; ^{13}C NMR (100 MHz, DMSO–d_6) δ: 14.8, (CH_3), 16.4 (CH_3), 29.1, 62.4, 64.1, 66.4, 114.1, 120.8, 124.8, 136.7,

143.2, 144.7, 150.8, 166.5 ppm; EI-MS: *m/z* = 340 [M^+]. Anal. Calc. for $C_{16}H_{20}N_8O$: C, 56.46; H, 5.92; N, 32.92. Found: C, 56.58; H, 5.77; N, 32.79%.

Synthesis of 2-methyl-5-((5-(2-(5-(2-(3-methyl-*1H*-benzo[4,5]imidazo[2,1-*c*][1,2,4]triazol-1-yl)ethyl)-*2H*-tetrazol-2-yl)ethyl)-*2H*-tetrazol-2-yl)methyl)-1,3,4-oxadiazole (7)

A mixture of compound **5** (4.36 g, 10 mmol), glacial acetic acid (6 mL), and acetic anhydride (3 mL) was heated under reflux for 4 hours. After concentration and cooling, the mixture was poured onto crushed ice. The resulting precipitate was filtered, dried, and recrystallized from DMF, affording a yellow powder (88%), m.p. > 300°C. IR (KBr) cm^{-1} ν_{max}: 2920 (CH aliphatic) and 1387 (C-O); ^{1}H NMR (300 MHz, DMSO-d_6): δ = 1.95 (3H, s, CH_3), 2.43 (3H, s, CH_3), 3.06 (4H, t, J = 5.5 Hz, $2CH_2$), 4.10 (4H, t, J = 4.2 Hz, $2CH_2$), 4.63 (2H, s, CH_2), 7.24-8.54 (4H, m, Ar-H) ppm; EI-MS: *m/z* = 460 [M^+]. Anal. Calc. for $C_{19}H_{20}N_{14}O$: C, 49.56; H, 4.38; N, 42.59. Found C, 49.69; H, 4.51; N, 42.71%.

Synthesis of 5-((5-(2-(5-(2-(3-methyl-*1H*-benzo[4,5]imidazo[2,1-*c*][1,2,4]triazol-1-yl)ethyl)-*2H*-tetrazol-2-yl)ethyl)-*2H*-tetrazol-2-yl)methyl)-1,3,4-oxadiazole-2-thiol (8)

Compound **5** (4.36 g, 10 mmol) and potassium hydroxide (1.68 g, 30 mmol) were dissolved in dimethylformamide (10 mL) and heated under reflux for 30 minutes. After cooling, carbon disulfide (3.15 mL, 40 mmol) was added, and the mixture was refluxed for 8 hours. The concentrated mixture was then cooled, poured onto crushed ice, and the resulting precipitate was filtered, dried, and recrystallized from DMF, affording a brown powder (59%), m.p. > 300°C. IR (KBr) cm^{-1} ν_{max}: 2951 cm^{-1} (CH aliphatic), 1624 cm^{-1} (C=N); ^{1}H NMR (300 MHz, DMSO-d_6): δ = 1.90 (3H, s, CH_3), 3.06 (4H, t, J = 5.5 Hz, $2CH_2$), 4.10 (4H, t, J = 4.2 Hz, $2CH_2$), 4.63 (2H, s, CH_2), 6.91-7.93 (4H, m, Ar-H), 12.46 (1H, s, SH) ppm; EI-MS: *m/z* = 478 [M^+]. Anal. Calc. for $C_{18}H_{18}N_{14}OS$: C, 45.18; H, 3.79; N, 40.98; S, 6.70. Found: C, 45.33; H, 3.95; N, 41.10; S, 6.85%.

Synthesis of 2-(2-(5-(2-(5-(2-(3-methyl-*1H*-benzo[4,5]imidazo[2,1-*c*][1,2,4]triazol-1-yl)ethyl)-*2H*-tetrazol-2-yl)ethyl)-*2H*-tetrazol-2-yl)acetyl)-*N*-phenylhydrazine carbothioamide (9)

Compound **5** (4.36 g, 10 mmol) and phenylisothiocyanate (1.35 g, 10 mmol) were dissolved in dimethylformamide (10 mL) and heated under reflux for 12 hours. After cooling, the solvent was concentrated under reduced pressure. The resulting residue was filtered, dried, and recrystallized from DMF, affording a brown powder (85%), m.p. > 300°C. IR (KBr) cm^{-1} ν_{max}: 3426 cm^{-1} (NH), 2951 cm^{-1} (CH aliphatic), 1635 cm^{-}1 (C=O); ^{1}H NMR (300 MHz, DMSO-d_6): δ = 1.97 (3H, s, CH_3), 3.06 (4H, t, J = 5.5 Hz, $2CH_2$), 4.10 (4H, t, J = 4.2 Hz, $2CH_2$), 4.63 (2H, s, CH_2), 6.48-7.91 (9H, m, Ar-H), 9.05 (1H, s, NH), 9.54 (1H, brs, NH), 10.12 (1H, brs, NH) ppm; EI-MS: m/z = 571 [M^+]. Anal. Calc. for $C_{24}H_{25}N_{15}OS$: C, 50.43; H, 4.41; N, 36.76; S, 5.61. Found C, 50.56; H, 4.53; N, 36.65; S, 5.74%.

Synthesis of *N*-(2-(2-(5-(2-(5-(2-(3-methyl-*1H*-benzo[4,5]imidazo[2,1-*c*][1,2,4]triazol-1-yl)ethyl)-*2H*-tetrazol-2-yl)ethyl)-*2H*-tetrazol-2-yl)acetyl)hydrazinecarbonothioyl) benzamide (10)

Compound **5** (4.36 g, 10 mmol) and benzoyl isothiocyanate (1.63 g, 10 mmol) were dissolved in dimethylformamide (10 mL) and heated under reflux for 12 hours. After cooling, the solvent was concentrated under reduced pressure. The resulting residue was filtered, dried, and recrystallized from DMF, producing a brown powder (80%), m.p. > 300°C. IR (KBr) cm^{-1} vmax: 3426 cm^{-1} (NH), 2951 cm^{-1} (CH), 1635 cm^{-1} (C=O); ^{1}H NMR (300 MHz, DMSO-d_6): δ = 1.97 (3H, s, CH_3), 3.10 (4H, t, J = 5.5 Hz, $2CH_2$), 4.15 (4H, t, J = 4.2 Hz, $2CH_2$), 4.62 (2H, s, CH_2), 7.11-8.56 (9H, m, Ar-H), 9.00 (1H, s, NH), 9.50 (1H, brs, NH), 10.12 (1H, brs, NH) ppm; EI-MS: m/z = 599 [M^+]. Anal. Calc. for $C_{25}H_{25}N_{15}O_2S$: C, 50.08; H, 4.20; N, 35.04; S, 5.35. Found C, 49.95; H, 4.32; N, 35.17; S, 5.48%.

Synthesis of 3-amino-5-((5-(2-(5-(2-(3-methyl-*1H*-benzo[4,5]imidazo[2,1-*c*][1,2,4]triazol-1-yl)ethyl)-*2H*-tetrazol-2-yl)ethyl)-*2H*-tetrazol-2-yl)methyl)-*4H*-pyrazole-4-carbonitrile (11)

Compound **5** (4.36 g, 10 mmol) and malononitrile (0.66 g, 10 mmol) were dissolved in dimethylformamide (10 mL) and heated under reflux for 6 hours. After cooling, the solvent was evaporated under reduced pressure, and the resulting precipitate was recrystallized from DMF, yielding a brown powder (86%), m.p. > 300°C. IR (KBr) cm^{-1} ν_{max}: 3422, 3455 cm^{-1} (NH_2), 2951 cm^{-1} (CH), 2314 cm^{-1}(CN), 1711 cm^{-1} ; ^{1}H NMR (300 MHz, DMSO-d_6): δ = 1.95 (3H, s, CH_3), 3.12 (4H, t, J = 5.5 Hz, $2CH_2$), 4.15 (4H, t, J = 4.2 Hz, $2CH_2$), 5.10 (2H, s, CH_2), 6.81-7.74 (4H, m, Ar-H), 8.05 (1H, s, CH), 12.05 (2H, brs, NH_2) ppm; EI-MS: m/z = 484 [M^+]. Anal. Calc. for $C_{20}H_{20}N_{16}$: C, 49.58; H, 4.16; N, 46.26. Found C, 49.73; H, 4.04; N, 46.15%.

2.2. Docking Study:

Ligand Preparation: The newly synthesized molecules were drawn using ChemDraw Professional 16.0, and molecular modeling was performed with software from the Molecular Operating Environment (MOE). Minimization was carried out until a root mean square deviation (RMSD) gradient of 0.1 kcal·mol^{-1}·Å^{-1} was reached using the MMFF 94× (Merck Molecular Force Field 94×). The oriented compounds were then saved in MDB format to facilitate the docking process [58].

Protein Preparation: The X-ray crystal structure of the enzyme (PDB ID: 8GVZ, resolution: 1.97 Å) was downloaded from the Protein Data Bank [59]. To prepare the enzyme for docking: (1) Only the URF co-crystallized ligand was retained, and crystallographic water molecules were removed. (2) Hydrogen atoms were added, broken bonds were reconnected, and the potential was corrected [60]. (3) Dummy atoms were generated using Alpha Site Finder for large site search. (4) The binding pocket was identified. (5) The pocket was saved in MOE format for modeling ligand-enzyme interactions. **Figure 1** shows the prepared protein.

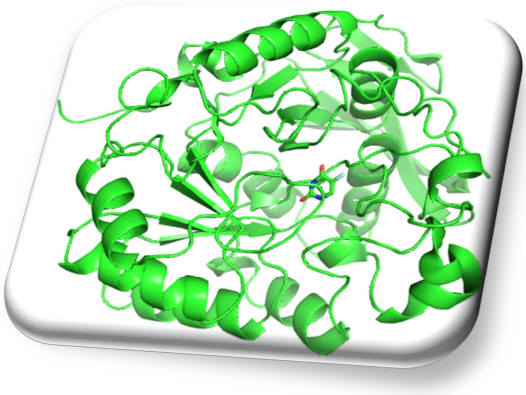

Figure 1: Prepared target protein, showing the crystal structure of the human dihydroorotase domain in complex with the anticancer drug 5-fluorouracil.

After docking, both 2D and 3D interactions with the amino acid residues were visualized. This study offers a solid introduction to 3D structure visualization and computational drug design using PyMOL [61]. PyMOL is available under an unrestricted open-source software license [62]. The interactions between the ligand and the active site amino acids were analyzed, and all docking procedures and scoring were documented according to established protocols [63].

2.3. In Silico Pharmacokinetic Profile (ADMET):

The pharmacokinetic profiles of key synthesized compounds were predicted using pkCSM [64]. This publicly accessible web server (http://structure.bioc.cam.ac.uk/pkcsm, accessed on 17 September 2024) provides a robust platform for the rapid evaluation of pharmacokinetic and toxicity properties [65]. Predicting the ADMET-related features of novel compounds involves correlating their pharmacokinetic and toxicological characteristics [66].

2.4. Evaluation of Cytotoxic Activity:

For the cytotoxicity assay, cells were seeded into 96-well plates at a density of 1×10^4 cells per well in 100 µL of growth medium. After 24 hours, a new medium containing serially diluted test compound concentrations was added using a multichannel pipette. Each concentration was tested in triplicate. Control wells included cells treated with and without DMSO to ensure DMSO levels (up to 0.1%) did not affect the results. Cell viability was measured colorimetrically. After incubation, 1% crystal violet was added for 30 minutes, followed by rinsing and the addition of 30% glacial acetic acid. Absorbance at 490 nm was measured using a TECAN microplate reader. Background absorbance was subtracted, and treated samples were compared to untreated controls [67]. Viability was calculated as [(OD_t/OD_c) \times 100%], where (OD_t) is the optical density of treated wells, and (OD_c) is that of controls. IC_{50} values were determined using dose-response curves in GraphPad Prism (San Diego, CA, USA) [57]

3. Results and Discussion

3.1. Chemistry

Tetrazole compound **1** was reacted with acrylonitrile in dry N,N-dimethylformamide under reflux to yield cyanoethyl tetrazole derivative **2** with a 60% yield. IR spectra confirmed aromatic C–H at 3058 cm^{-1}, aliphatic C–H at 2927 cm^{-1}, and a CN stretch at 2373 cm^{-1}. Mass spectrometry showed a molecular ion peak at m/z 321 [M^+]. In the ^1H NMR spectrum, a singlet at 2.12 ppm corresponded to the CH_3 group, while triplets at 3.00, 3.20, 4.05, and 4.12 ppm represented methylene protons. Aromatic protons appeared as multiplets between 6.95–7.85 ppm.

Compound **2** was then reacted with sodium azide and ammonium chloride in dry N,N-dimethylformamide under reflux to produce the corresponding tetrazole compound 3 with a 63% yield (**Scheme 1**). IR spectra indicated the disappearance of the CN group and the appearance of an NH group at 3426 cm^{-1}. ^1H NMR spectra showed a singlet peak at 1.95 ppm for the CH_3 group, four triplet peaks in the region of 3.00–4.04 ppm for the CH_2 groups, multiplet peaks from 6.93 to 7.85 ppm for aromatic protons, and a broad peak at 9.10 ppm for the NH group. Mass spectra showed a molecular ion peak at m/z 364 [M^+].

The bis-tetrazole **3** was stirred with ethyl chloroacetate and potassium carbonate in dry N,N-dimethylformamide at room temperature, yielding ester derivative **4** with a 56% yield (**Scheme 1**). The IR spectrum indicated the disappearance of the NH absorption at 3426 cm^{-1}. The ^1H NMR spectrum showed a triplet for a CH_3 group at 1.24 ppm, a singlet for a CH_3 group at 1.95 ppm, triplet peaks for CH_2 groups in the range of 3.00–4.04 ppm, a quartet for a CH_2 group at 4.12 ppm, and a multiplet for aromatic protons in the region of 6.75–7.82 ppm. The mass spectrum displayed a molecular ion peak at m/z 450 [M^+].

The acid hydrazide derivative **5** was obtained in 63% yield by refluxing compound **4** with hydrazine hydrate in dry N,N-dimethylformamide (**Scheme 1**). Its structure was supported by spectroscopic data: the IR spectrum exhibited bands indicative of NH_2 (3422, 3450 cm^{-1}), NH (3334 cm^{-1}), and carbonyl (CO, 1687 cm^{-1}) functionalities. The ^1H NMR spectrum revealed a methyl singlet at 1.95 ppm, a broad amine peak at 2.43 ppm, methylene triplets in the range of 3.00–4.04 ppm, aromatic proton multiplets between 6.75 and 7.82 ppm, and an amide NH signal at 8.56 ppm. The molecular ion peak in the mass spectrum was observed at m/z 436 [M^+].

The reaction of tetrazole compound **1** with 1-bromo-2-ethoxyethane was conducted in anhydrous DMF under reflux conditions, resulting in the formation of compound **6** in 81% yield (**Scheme 1**). Characterization by IR spectroscopy revealed the disappearance of the NH band and the appearance of a C-O stretching vibration at 1387 cm^{-1}. The ^1H NMR spectrum displayed signals including a triplet at δ 1.12 ppm (CH_3), a singlet at δ 1.95 ppm (CH_3), triplets between δ 3.00 and 4.04 ppm (CH_2), a quartet at δ 3.85 ppm (CH_2), and multiplets in the range of δ 7.22–8.24 ppm (aromatic protons). The mass spectrum exhibited a molecular ion [M^+] at m/z 340.

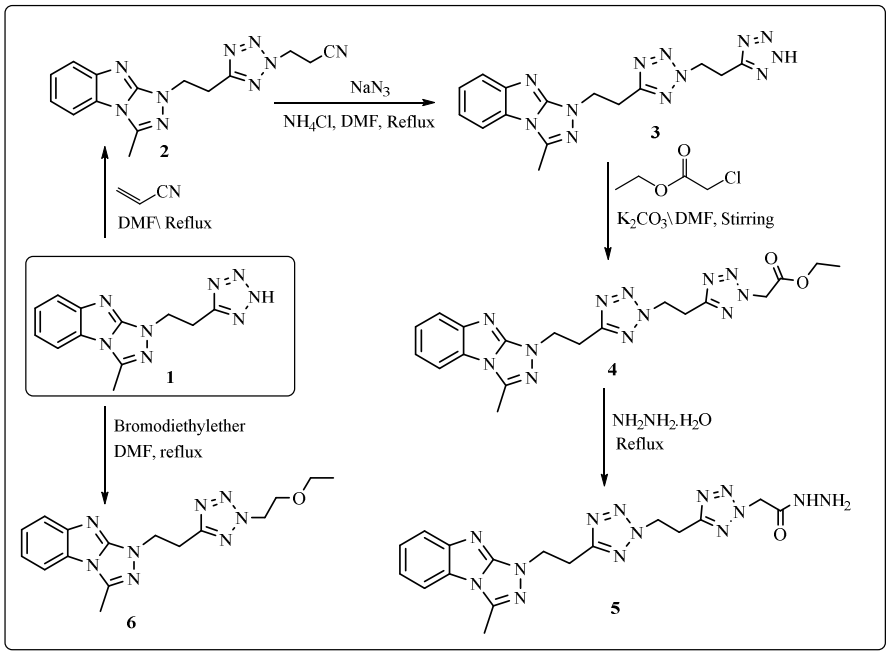

Scheme 1. Synthesis of triazolobenzoimidazole-tetrazole hybrid derivatives **2-6**

Under reflux conditions, acid hydrazide **5** was treated with the following reagents to afford derivatives **7–11**: acetic anhydride in acetic acid (88%), carbon disulfide and potassium hydroxide in anhydrous N,N-dimethylformamide (59%), phenylisothiocyanate in anhydrous N,N-dimethylformamide (85%), benzoylisothiocyanate in anhydrous N,N-dimethylformamide (80%), and malononitrile in anhydrous N,N-dimethylformamide (86%) (**Scheme 2**). Spectroscopic data for compound **7** included an IR spectrum indicating the loss of the NH_2 group and the presence of C-O (1387 cm^{-1}) and aliphatic C-H (2920 cm^{-1}) stretches. The ^1H NMR spectrum exhibited signals at δ 1.95 ppm (s, 3H, CH_3), δ 2.43 ppm (s, 3H, CH_3), δ 3.06–4.10 ppm (m, several CH_2), δ 4.63 ppm (s, 2H, CH_2), and δ 7.24–8.54 ppm (m, aromatic H). The mass spectrum confirmed the molecular weight with an [M^+] ion at m/z 460. The IR spectrum of compound 8 indicated the absence of an N-H stretching band. The ^1H NMR spectrum showed characteristic signals at δ 1.90 ppm (CH_3 singlet), δ 2.43 ppm (CH_3 singlet), δ 3.06–4.10 ppm (CH_2 triplets), δ 4.63 ppm (CH_2 singlet), δ 6.91–7.93 ppm (aromatic multiplets), and δ 12.46 ppm (SH singlet). The mass spectrum exhibited a molecular ion peak [M^+] at m/z 478. The IR spectrum of compound 9 showed characteristic absorptions for an N-H stretching band at 3426 cm^{-1} and carbonyl (C=O) stretching at 1635 cm^{-1}. The ^1H NMR spectrum exhibited signals at δ 1.97 ppm (CH_3 singlet), δ 3.06–4.10 ppm (CH_2 triplets), δ 4.63 ppm (CH_2 singlet), δ 6.48–7.91 ppm (aromatic multiplets), and broad N-H signals around δ 9.05, 9.54, and 10.12 ppm. The mass spectrum displayed a molecular ion peak [M^+] at m/z 571. Compound 10 showed IR absorptions for an N-H stretching band at 3428 cm^{-1} and carbonyl (C=O) stretching at 1637 cm^{-1}. The ^1H NMR spectrum featured signals at δ 1.97 ppm (CH_3 singlet), δ 3.10–4.15 ppm (CH_2 triplets), δ 4.62 ppm (CH_2 singlet), δ 7.11–8.56 ppm (aromatic multiplets), and broad N-H signals around δ 9.00, 9.50, and 10.12 ppm. The mass spectrum showed a molecular ion peak [M^+] at m/z 599. For compound **11**, the mass spectrum showed a molecular ion peak [M^+] at m/z 484. The IR spectrum identified N-H stretching bands at 3422 and 3455 cm^{-1}, aliphatic C-H stretching at 2951 cm^{-1}, and cyano (C≡N) stretching at 2314 cm^{-1}. The ^1H NMR spectrum showed signals at δ 1.95 ppm (CH_3 singlet), δ 3.12–4.15 ppm (CH_2 triplets), δ 5.10 ppm (CH_2 singlet), δ 6.81–7.74 ppm (aromatic multiplets), a C-H singlet at δ 8.05 ppm, and a broad NH_2 signal at δ 12.05 ppm (**Scheme 2**).

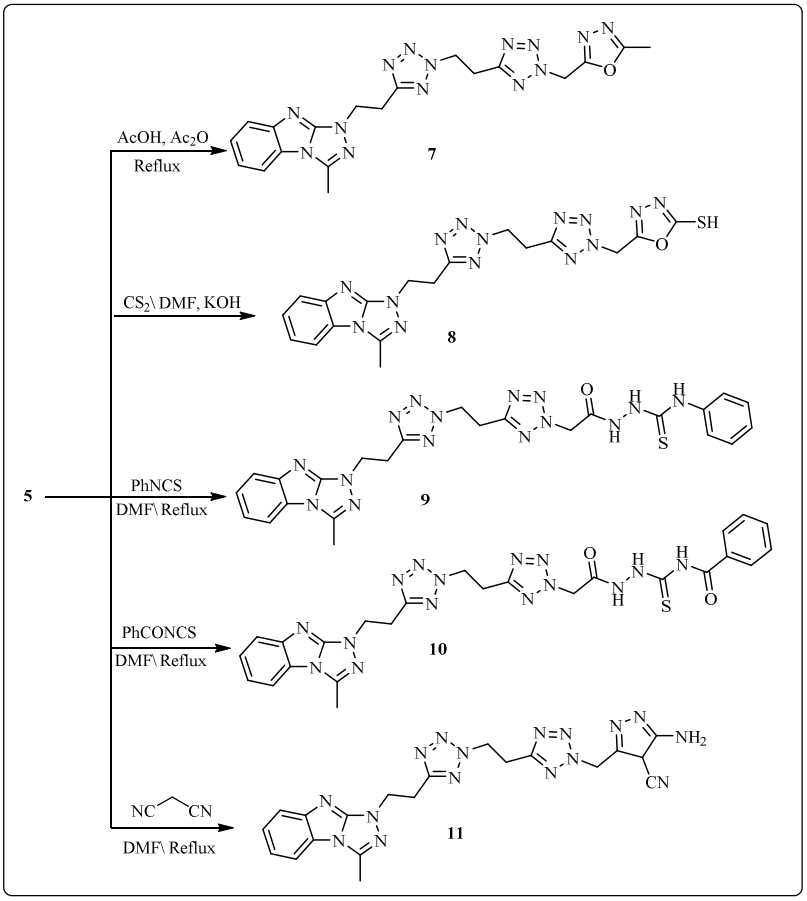

Scheme 2. Synthesis of triazolobenzoimidazole-tetrazole hybrid derivatives **7-11**

3.2 Molecular docking study:

The crystal structure of the human dihydroorotase domain complexed with the anticancer drug 5-fluorouracil (PDB ID: 8GVZ) was obtained from the Protein Data Bank [59]. Molecular docking was employed to explore the binding interactions between the target anticancer protein and the ligands. This computational technique helped identify how the ligands interact with the active site of the target protein [68]. PyMOL, an open-source tool for biomolecule visualization, was used due to its ease of use, extensive documentation, widespread adoption, and high-quality rendering features [69, 70]. Docking results were compared with the binding energy of 5-FU, the co-crystallized ligand. Key findings include: (i) The binding energies of the novel ligands were more negative than those of the co-crystallized ligand, indicating greater stability. (ii) Interactions included various types, such as hydrogen bond donors, π-π interactions, hydrogen bond acceptors, hydrogen-π interactions, and π-hydrogen interactions. (iii) Critical binding residues included Asp1796, Trp1758, Thr1782, Val1783, Asp1753, His1756, Tyr1794, Ala1494, His1763, Lys1460, and Thr1759. (iv) Key ligation sites involved atoms such as nitrogen, sulfur, carbon, and oxygen within the benzimidazolo-triazole tetrazole scaffold. As shown in **Table 1**, compound **1** formed a hydrogen bond between Asp1796 and the nitrogen atom of the tetrazole ring. **Figure 2** highlights that compound **3** formed a hydrogen bond with Asp1753. Further docking analysis revealed that compounds **2** and **5** acted as hydrogen bond acceptors with Thr1782, involving the nitrogen atoms of the triazole and imidazole rings, respectively. Additionally, compound **2** formed another hydrogen bond acceptor interaction between its cyano group and Val1783, while compound **5** formed a similar interaction between its tetrazole nitrogen and Tyr1794. In the 2D model of compound **8**, a hydrogen bond donor interaction was observed between the sulfur atom and Ala1494, while the 3D model of compound **9** showed a hydrogen bond acceptor interaction between the tetrazole nitrogen and Tyr1794. Compound **10** displayed a hydrogen bond donor interaction between its nitrogen atom and Lys1460, and compound **11** featured a hydrogen bond acceptor interaction between Thr1782 and the oxygen atom of its carbonyl group. As shown in **Table 1**, compound **1** formed an H-bond between Asp1796 and the nitrogen atom of the tetrazole ring. **Figure 1** highlights that compound **3** formed an H-bond with Asp1753. Further docking analysis revealed that compounds **2** and **5** formed H-bond acceptors with Thr1782, involving the nitrogen atoms of the triazole and imidazole rings, respectively. Additionally, compound **2** formed another H-bond acceptor between its cyano group and Val1783, while compound **5** formed a similar interaction between its tetrazole nitrogen and Tyr1794. In the 2D model of compound **8**, an H-bond donor was observed between the sulfur atom and Ala1494, while the 3D model of compound **9** showed an H-bond acceptor between the tetrazole nitrogen and Tyr1794. Compound **10** displayed an H-bond donor interaction between its

nitrogen atom and Lys1460, and compound **11** featured an H-bond acceptor between Thr1782 and the oxygen atom of its carbonyl group. Consistent with docking scores, compounds **11, 9, 5, 4,** and **7** showed the highest anticancer activity in MCF-7 cell assays.

Table 1. Docking score (kcal/mol), number of hydrogen bonds, and number of arene interactions of novel synthesized compounds (**1-11**) with the 8GVZ receptor, relative to 5-FU.

Cpd. NO.	Docking score (kcal/mol)	NO. of hydrogen bonding	Donor atom	Acceptor atom	NO. of arene interaction
1	-5.83	1 (Asp1796)	N	-	2 (π- π) [Trp1758]
2	-6.54	1 (Val1783) 1 (Thr1782)	-	N	-
3	-6.61	1 (Asp1753)	N	-	1 (π-π) [His1756]
4	-7.11	-	-	-	-
5	-7.18	1 (Tyr1794) 1 (Thr1782)	-	N	-
6	-6.33	-	-	-	-
7	-7.05	-	-	-	-
8	-6.89	1 (Ala1494)	S	-	1 (H-π) [His1756]
9	-7.58	1 (Tyr1794)	-	N	1 (H-π) [His1763]
10	-6.80	1 (Lys1460)	N	-	1 (H-π) [His1756]
11	-8.14	1 (Thr1782)	-	O	2 (π-*H*) [Thr1759]
5-FU	-4.20	-	-	-	-

Cpd. NO.	3D Ligand interaction	2D Ligand interaction
1	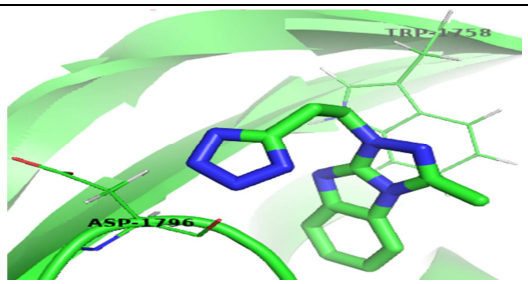	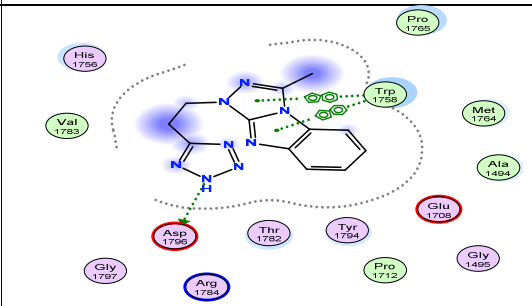
2	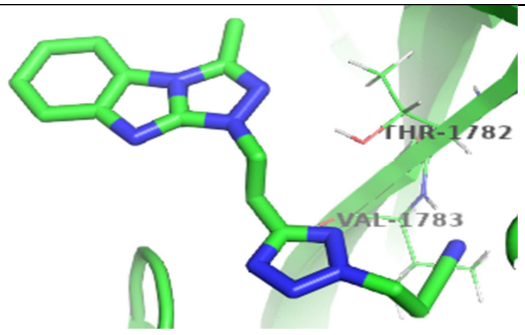	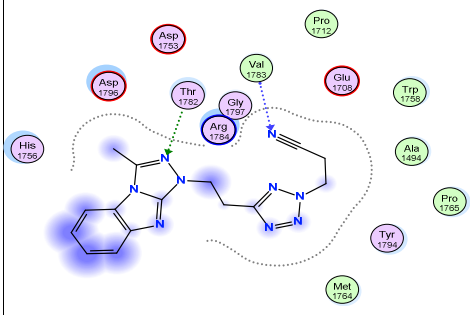

3	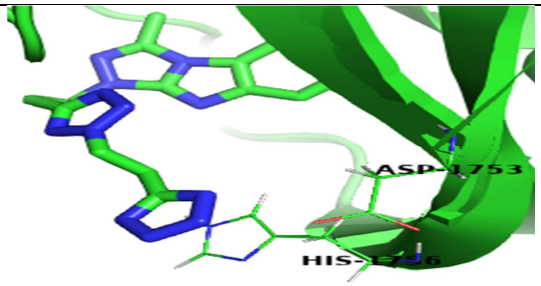	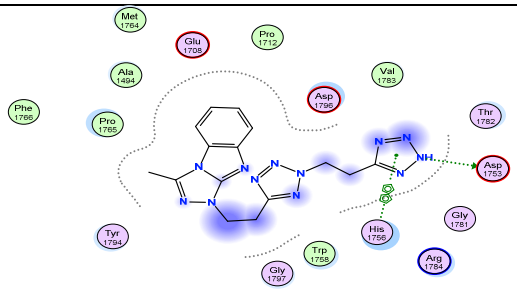
4	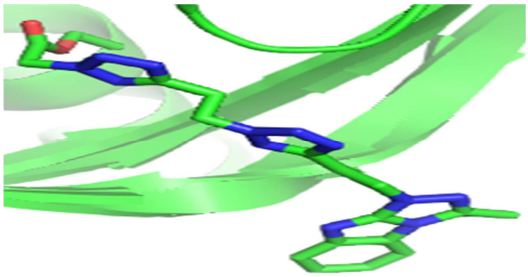	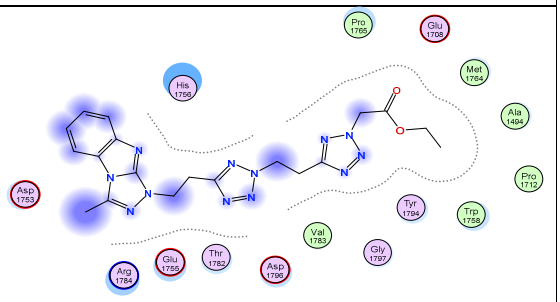
5	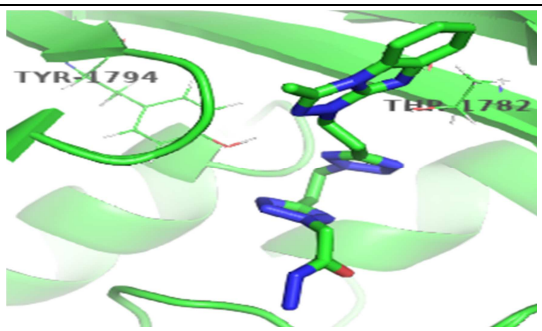	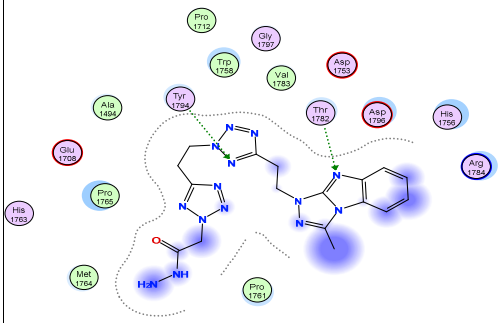
6	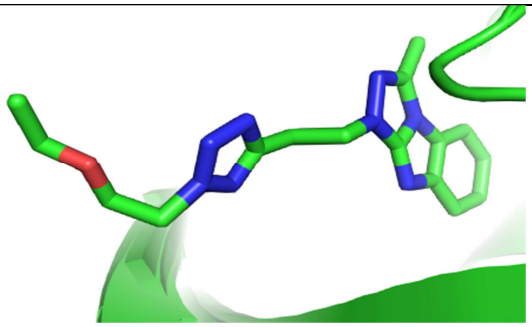	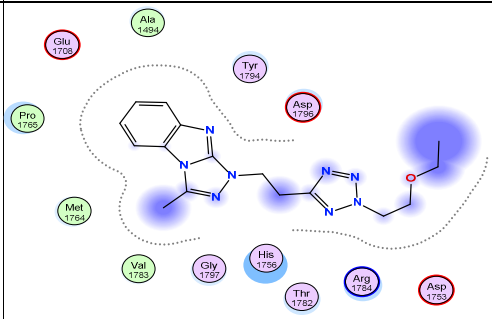
7	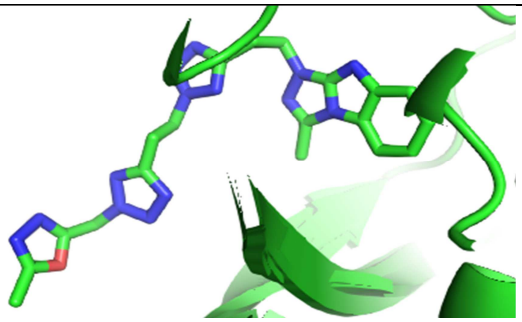	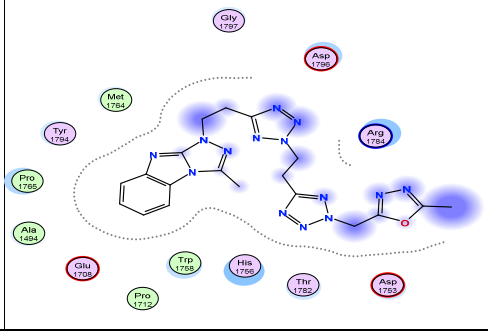

8	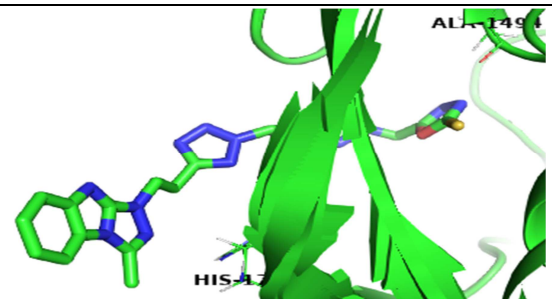	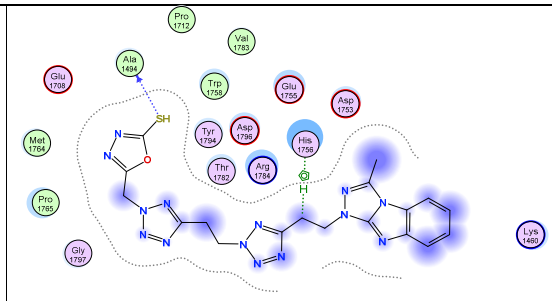
9	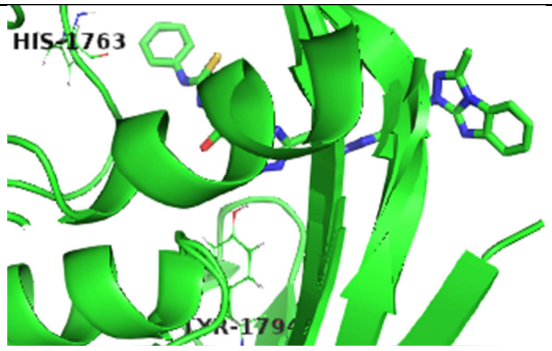	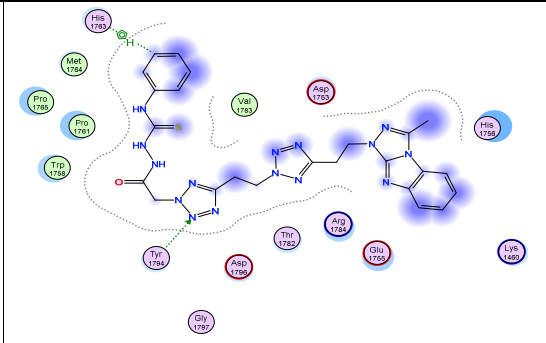
10	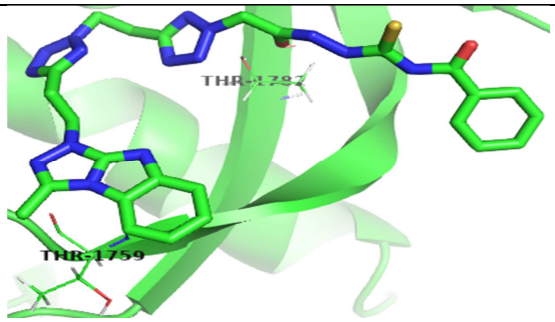	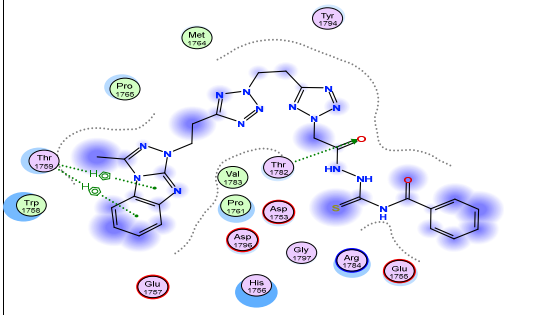
11	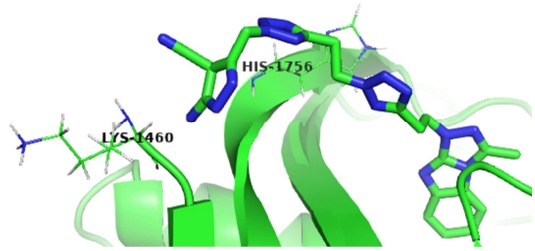	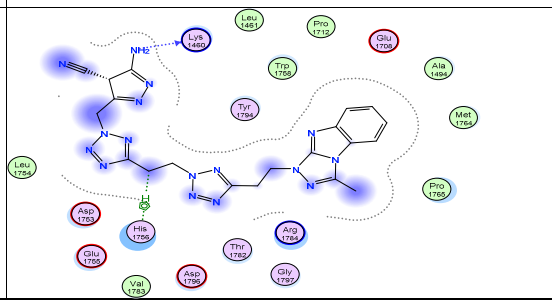

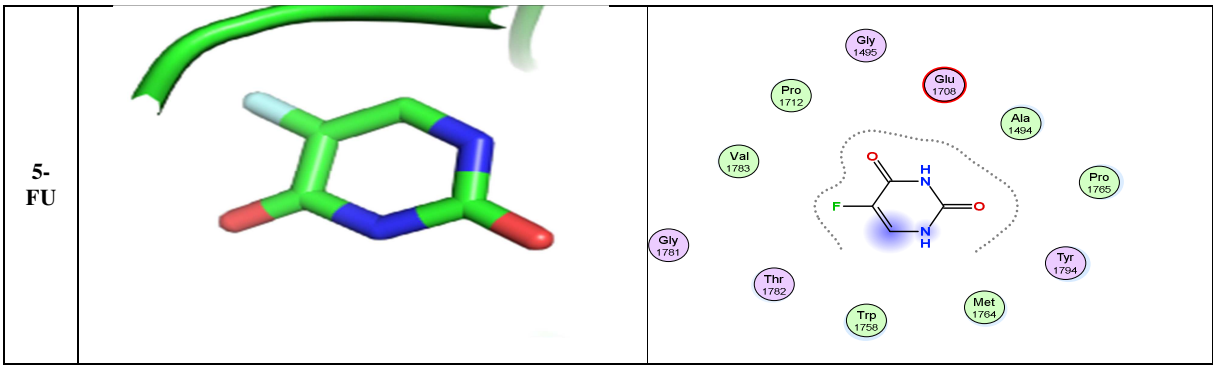

Figure 2: 3D and 2D representations of ligand interactions within the 8GVZ binding site for novel synthesized compounds (**1-11**).

3.2. In silico pharmacokinetic profile (ADMET):

The average absorption percentage of the tested novel compounds through the human intestine ranged from 60.16% to 93.90%. Regarding distribution, compounds that do not target the central nervous system (CNS) should have minimal CNS penetration to avoid adverse effects; the evaluated compounds showed a log PS between -4.14 and -2.84. In terms of metabolism, compounds **1-11** inhibited the CYP3A4 substrate, while compounds **1, 2,** and **6** could also be metabolized by the CYP1A2 inhibitor. Additionally, compounds 9 and 10 inhibited CYP3A4. The excretion of these compounds, measured as a log value in ml/min/kg, ranged from 0.20 to 1.01. All these data are summarized in **Table 2**. Toxicity predictions further indicated that none of the tested compounds caused skin sensitization.

Table 2. ADMET properties of novel synthetic compounds (**1-11**).

Cpd. NO.	Absorption	Distribution	Metabolism	Excretion [Log ml/min/kg]	Toxicity
	Intestinal absorption (human) [% Absorbed]	CNS permeability (log PS)			Skin Sensitization [Yes/No]
1	60.16	-2.85	CYP3A4 Substrate; & CYP1A2 Inhibitor	0.74	No
2	93.90	-2.84		0.87	
3	79.20	-3.74	CYP3A4 Substrate	0.69	
4	86.86	-3.90		0.80	
5	72.04	-4.14		0.6	
6	88.58	-3.31	CYP3A4 Substrate; & CYP1A2 Inhibitor	1.01	
7	92.16	-3.83	CYP3A4 Substrate	0.52	
8	86.89	-3.90		0.41	
9	73.76	-3.82	CYP3A4 Substrate; & CYP3A4 Inhibitor	0.42	
10	69.20	-4.00		0.35	
11	81.79	-3.96	CYP3A4 Substrate	0.20	
5-FU	88.82	-3.05	-	0.62	

3.3. Anticancer Activity

The inhibitory effects and IC_{50} values of the most active newly synthesized compounds **4**, **5**, **7**, **9**, and **11** were tested against MCF-7 breast cancer cells using the MTT viability assay, with 5-fluorouracil (5-FU) serving as a reference standard. Dose-response curves were generated to determine the IC_{50}, which is the concentration required to inhibit cell growth by 50%. The cytotoxic activity of each compound was evaluated by calculating the average IC_{50} values from three independent experiments to ensure reliable data. The results revealed a highly significant difference ($p < 0.001$) in the inhibitory effects of the compounds across varying concentrations, demonstrating a clear dose-dependent response. These effects were systematically compared to those of 5-FU, highlighting distinct levels of growth inhibition among the compounds. The detailed statistical analysis and graphical representations of these findings are presented in **Table 3** and **Figure 3**.

Table 3. Cytotoxicity (IC_{50} μM) of compounds **4, 5, 7, 9**, and **11** against MCF-7 cell lines.

Compounds no	IC_{50} (μM)
5-FU	*0.11 ± 0.3*
4	*0.59 ± 0.7*
5	0.53 ± *1.0*
7	*0.92 ± 0.7*
9	0.47 ± *0.5*
11	*0.21 ± 0.4*

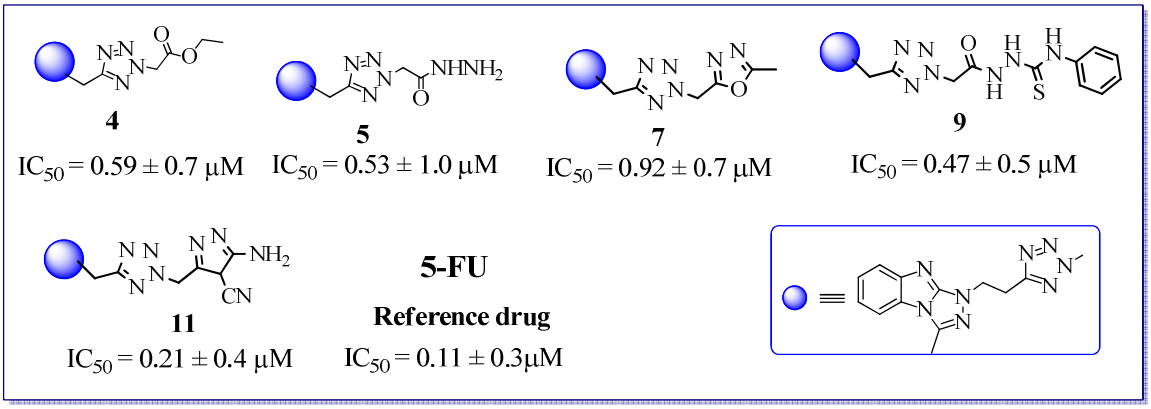

Figure 3: SAR of compounds **4, 5, 7, 9**, and **11** as anticancer agents.

4. Conclusion

In this study, a series of benzimidazolo-triazole-tetrazole derivatives was synthesized and structurally characterized. Molecular docking and ADMET profiling identified compounds **4, 5, 7, 9,** and **11** as promising candidates, with compound **11** showing the most potent in vitro cytotoxicity against MCF-7 cells. These results support their potential as anticancer agents. Future work will focus on structural optimization and in vivo studies to further assess their therapeutic efficacy and safety.

Conflicts of Interest

The authors declare no conflicts of interest.

Formatting of funding sources

There is no funding

5. References and Bibliography

[1] Kabir, E.; Uzzaman, M. A Review on Biological and Medicinal Impact of Heterocyclic Compounds. Results Chem. 2022, 4, 100606.

[2] Nishanth Rao, R.; Jena, S.; Mukherjee, M.; Maiti, B.; Chanda, K. Green Synthesis of Biologically Active Heterocycles of Medicinal Importance: A Review. Environ. Chem. Lett. 2021, 19, 3315–3358.

[3] Farag, B.; Zaki, M. E. A.; Elsayed, D. A.; Gomha, S. M. Benzimidazole Chemistry in Oncology: Recent Developments in Synthesis, Activity, and SAR Analysis. RSC Adv. 2025, 15, 18593.

[4] Marinescu, M. Synthesis of Antimicrobial Benzimidazole–Pyrazole Compounds and Their Biological Activities. Antibiotics 2021, 10, 1002.

[5] Raducka, A.; Świątkowski, M.; Korona-Głowniak, I.; Kapron, B.; Plech, T.; Szczęsio, M.; Gobis, K.; Szynkowska-Jóźwik, M. I.; Czylkowska, A. Zinc Coordination Compounds with Benzimidazole Derivatives: Synthesis, Structure, Antimicrobial Activity and Potential Anticancer Application. Int. J. Mol. Sci. 2022, 23, 6595.

[6] Al-Saleem, M. S. M.; Ahmed, M. S. M.; Riyadh, S. M.; Alruwaili, A. H.; Zaki, M. E. A.; Gomha, S. M. Synthesis, Molecular Characterization, and Antimicrobial Evaluation of Hydrazones Derived from 2-Hydrazinobenzimidazole. Drug Des. Dev. Ther. 2025, 19, 4437–4456.

[7] Lee, Y. T.; Tan, Y. J.; Oon, C. E. Benzimidazole and Its Derivatives as Cancer Therapeutics: The Potential Role from Traditional to Precision Medicine. Acta Pharm. Sin. B 2023, 13, 478–497.

[8] Song, B.; Park, E. Y.; Kim, K. J.; Ki, S. H. Repurposing of Benzimidazole Anthelmintic Drugs as Cancer Therapeutics. Cancers 2022, 14, 4601.

[9] Natarajan, R.; Kumar, P.; Subramani, A.; Siraperuman, A.; Angamuthu, P.; Bhandare, R. R.; Shaik, A. B. A Critical Review on Therapeutic Potential of Benzimidazole Derivatives: A Privileged Scaffold. MedChem 2024, 20(3), 311–351.

[10] Othman, D. I. A.; Hamdi, A.; Tawfik, S. S.; Elgazar, A. A.; Mostafa, A. S. Identification of New Benzimidazole-Triazole Hybrids as Anticancer Agents: Multi-Target Recognition, In Vitro and In Silico Studies. J. Enzyme Inhib. Med. Chem. 2023, 38, 2166037.
[11] Nawareg, N. A.; Mostafa, A. S.; El-Messery, S. M.; Nasr, M. N. A. New Benzimidazole Based Hybrids: Synthesis, Molecular Modeling Study and Anticancer Evaluation as Topo II Inhibitors. Bioorg. Chem. 2022, 127, 106038.
[12] Sović, I.; Jambon, S.; Pavelić, S. K.; Markova-Car, E.; Ilić, N.; Depauw, S.; David-Cordonnier, M.-H.; Karminski-Zamola, G. Synthesis, Antitumor Activity and DNA Binding Features of Benzothiazolyl and Benzimidazolyl Substituted Isoindolines. Bioorg. Med. Chem. 2018, 26(8), 1950–1960.
[13] Sheng, C.; Miao, Z.; Zhang, W. New Strategies in the Discovery of Novel Non-Camptothecin Topoisomerase I Inhibitors. Curr. Med. Chem. 2011, 18(28), 4389–4409.
[14] Galal, S. A.; Hegab, K. H.; Hashem, A. M.; Youssef, N. S. Synthesis and Antitumor Activity of Novel Benzimidazole-5-Carboxylic Acid Derivatives and Their Transition Metal Complexes as Topoisomerase II Inhibitors. Eur. J. Med. Chem. 2010, 45(12), 5685–5691.
[15] Shrouk, A.; Magda, A.; Abdallah, S.; Heba, S.; Salah, M. A.; Soliman, M.; Gomha, S.; Bassiony, H.; Rashdan, H. R. M. Chitosan (CS)/Polyvinyl Alcohol (PVA) Films Loaded with Novel Synthesized 1,2,3-Triazole Derivative for Cancer Treatment. Egypt. J. Chem. 2024, 67, 279–288.
[16] Alweet, M. N. D.; El-Bayaa, M.; Almendrej, M. F.; Gomha, M. S.; Alenazy, A.; Nossier, S. E.; El-Sayed, A. Wael. Synthesis, Molecular Docking and Anticancer Activity of New Pyridyl-1,2,4-Triazole-Thioglycosides and Their Pyridyl-[1,2,4]Triazolo[1,5-a]Pyridine-Glycoside Analogues. Egypt. J. Chem. 2024, 67, 1251–1260.
[17] Ramadan, R. S.; Gomha, S.; El-Helw, A. E.; Eman, S. In Silico ADME, DFT, and Antiproliferative Activity of Pyrazole-Based Pyrimidinethione, Triazolethione, and Thiadiazolopyrimidine Derivatives. Russ. J. Gen. Chem. 2025, 95(2), 491–504.
[18] Abu-Melha, S.; Edrees, M. M.; Kheder, N. A.; Saad, A. M.; Riyadh, S. M.; Abdel-Aziz, M. M.; Abdelmoaz, M. A.; Gomha, M. S. Synthesis and Anti-Tubercular Evaluation of Bis-[4-Ethylidineamino[1,2,4]Triazole-3-Thiol] Tethered by 1,4-Dihydropyridine. Russ. J. Bioorg. Chem. 2022, 48(2), 345–352.
[19] Nora, N. S. A.; Al-Sahaly, S.; Ghannay, S.; Kaiss, A.; El-Bayaa, M. F.; Almendrej, M.; Gomha, M. S.; Elganzory, H. H.; El-Sayed, A. Wael. Synthesis, Molecular Docking and Anticancer Activity of New Substituted Pyridine-1,2,3-Triazole Hybrid N-Glycosides via Click Chemistry. Egypt. J. Chem. 2024, 67, 1221–1233.
[20] Abdulmohsen, S. A.; Altuwayjiri, A.; El-Ghoula, Y.; El-Sayed, A. Wael; Gomha, M. S. 1,2,3-Triazole-Based Chitosan Derivatives: Recent Aspects, Synthesis and Therapeutic Potential. Egypt. J. Chem. 2024, 67(13), 1317–1331.
[21] El-Sayed, W. A.; Alhaniny, A.; El Ghoul, Y.; Gomha, S. Cyclodextrin-Based Compounds and Their Derived 1,2,3-Triazoles: Recent Aspects, Synthesis, Overview and Applications. Egypt. J. Chem. 2024, 67(13), 1279–1305.
[22] Gomha, S. M.; Edrees, M. M.; Muhammad, Z. A.; Kheder, N. A.; Abu-Melha, S.; Saad, A. M. Synthesis, Characterization and Antimicrobial Evaluation of Some New 1,4-Dihydropyridines-1,2,4-Triazole Hybrid Compounds. Polycycl. Aromat. Compd. 2022, 42(1), 173–185.
[23] Hashem, H. E.; Amr, A. E.-G.-E.; Nossier, E. S.; Anwar, M. M.; Azmy, E. M. New Benzimidazole-1,2,4-Triazole- and 1,3,5-Triazine-Based Derivatives as Potential EGFRWT and EGFRT790M Inhibitors: Microwave-Assisted Synthesis, Anticancer Evaluation, and Molecular Docking Study. ACS Omega 2022, 7, 7155–7171.
[24] Güzel, E.; Çevik, U. A.; Evren, A. E.; Bostancı, H. E.; Gül, U. D.; Kayış, U.; Özkay, Y.; Kaplancıklı, Z. A. Synthesis of Benzimidazole-1,2,4-Triazole Derivatives as Potential Antifungal Agents Targeting 14α-Demethylase. ACS Omega 2023, 8, 4369–4384.
[25] Çevik, U. A.; Köy, B.; Celik, I.; Rudrapal, M.; Rakhit, G.; Kray, A.; Levent, ; Omeniy, D.; ğlık Ökten, B. N.; Bayal, M.; Eklioğlu, Ö. A.; Öksüz, Y.; Kaplancıklı, Z. A. New Benzimidazole-Triazole Derivatives as Topoisomerase I Inhibitors: Design, Synthesis, Anticancer Screening, and Molecular Modeling Studies. ACS Omega 2024, 9(11), 13359–13372.
[26] Marinescu, M. Benzimidazole-Triazole Hybrids as Antimicrobial and Antiviral Agents: A Systematic Review. Antibiotics (Basel) 2023, 12(7), 1220.
[27] Goud, N. S.; Pooladanda, V.; Chandra, K. M.; Soukya, P. S. L.; Alvala, R.; Kumar, P.; Nagaraj, C.; Bharath, R. D.; Qureshi, I. A.; Godugu, C.; Alvala, M. Novel Benzimidazole-Triazole Hybrids as Apoptosis Inducing Agents in Lung Cancer: Design, Synthesis, 18F-Radiolabeling & Galectin-1 Inhibition Studies. Bioorg. Chem. 2020, 102, 104125.
[28] Wang, S.-Q.; Wang, Y.-F.; Xu, Z. Tetrazole Hybrids and Their Antifungal Activities. Eur. J. Med. Chem. 2019, 170, 225–234.
[29] Asadi, M.; Mohammadi-Khanaposhtani, M.; Hosseini, F. S.; Gholami, M.; Dehpour, A. R.; Amanlou, M. Design, Synthesis, and Evaluation of Novel Racecadotril-Tetrazole-Amino Acid Derivatives as New Potent Analgesic Agents. Res. Pharm. Sci. 2021, 16(4), 341.
[30] Hatamleh, A. A.; Al Farraj, D.; Al-Saif, S. S.; Chidambaram, S.; Radhakrishnan, S.; Akbar, I. Synthesis, Cytotoxic Analysis, and Molecular Docking Studies of Tetrazole Derivatives via N-Mannich Base Condensation as Potential Antimicrobials. Drug Des. Devel. Ther. 2020, 14, 4477–4492.
[31] Dhiman, N.; Kaur, K.; Jaitak, V. Tetrazoles as Anticancer Agents: A Review on Synthetic Strategies, Mechanism of Action and SAR Studies. Bioorg. Med. Chem. 2020, 28(15), 115599.
[32] Wang, S.-Q.; Wang, Y.-F.; Xu, Z. Tetrazole Hybrids and Their Antifungal Activities. Eur. J. Med. Chem. 2019, 170, 225–234.

[33] Ramakrishna, V.; Sai Leela, R.; Ravindranath, L. K. Novel Route for Synthesis of Antihypertensive Activity of Tetrazole Analogues as Carbamate and Urea Derivatives. Med. Chem. (Los Angeles) 2017, 7, 239–246.
[34] Gomha, S. M.; Edrees, M. M.; El-Arab, E. E. Synthesis and Preliminary In Vitro Cytotoxic Evaluation of Some Novel Bis-Heterocycles Incorporating Thienothiophene. J. Heterocycl. Chem. 2017, 54, 641–647.
[35] Popova, E. A.; Protas, A. V.; Trifonov, R. E. Tetrazole Derivatives as Promising Anticancer Agents. Anticancer Agents Med. Chem. 2018, 17(14), 1856–1868.
[36] Zhang, J.; Wang, S.; Ba, Y.; Xu, Z. Tetrazole Hybrids with Potential Anticancer Activity. Eur. J. Med. Chem. 2019, 178, 341–351.
[37] Verma, A.; Kaur, B.; Venugopal, S.; Wadhwa, P.; Sahu, S.; Kaur, P.; Kumar, D.; Sharma, A. Tetrazole: A Privileged Scaffold for the Discovery of Anticancer Agents. Chem. Biol. Drug Des. 2022, 100(3), 419–442.
[38] Gorle, S.; Maddila, S.; Maddila, S. N.; Naicker, K.; Singh, M.; Singh, P.; Jonnalagadda, S. B. Synthesis, Molecular Docking Study and In Vitro Anticancer Activity of Tetrazole-Linked Benzochromene Derivatives. Anticancer Agents Med. Chem. 2017, 17(3), 464–470.
[39] Song, Y. N.; Zhan, P.; Liu, X. Heterocycle-Thioacetic Acid Motif: A Privileged Molecular Scaffold with Potent, Broad-Ranging Pharmacological Activities. Curr. Pharm. Des. 2013, 19(40), 7141–7154.
[40] Kitchen, D. B.; Decornez, H.; Furr, J. R.; Bajorath, J. Docking and Scoring in Virtual Screening for Drug Discovery: Methods and Applications. Nat. Rev. Drug Discov. 2004, 3(11), 935–949.
[41] Al-Humaidi, Y. A. J.; Albedair, L.; Maliwal, D.; Zaki, E. A. M.; Al-Hussain, A. S.; Pissurlenkar, R.; Mukhrish, E. M. Y.; Abolibda, Z. A. T.; Gomha, M. S. Synthesis and Molecular Docking of Curcumin-Derived Pyrazole-Thiazole Hybrids as Potent Inhibitors of α-Glucosidase. Chem. Biodiversity 2025, 22(2), e202401766.
[42] Li, A. P. Screening for Human ADME/Tox Drug Properties in Drug Discovery. Drug Discov. Today 2001, 6(7), 357–366.
[43] Lin, J.; Sahakian, D. C.; De Morais, S.; Xu, J. J.; Polzer, R. J.; Winter, S. M. The Role of Absorption, Distribution, Metabolism, Excretion and Toxicity in Drug Discovery. Curr. Top. Med. Chem. 2003, 3(10), 1125–1154.
[44] Zaki, Y. H.; Al-Gendey, M. S.; Abdelhamid, A. O. A Facile Synthesis, and Antimicrobial and Anticancer Activities of Some Pyridines, Thioamides, Thiazole, Urea, Quinazoline, β-Naphthyl Carbamate, and Pyrano[2,3-d]Thiazole Derivatives. Chem. Cent. J. 2018, 12(1), 1–14.
[45] Fouad, S. A.; El-Gendey, M. S.; Ahmed, E. M.; Hessein, S. A.; Ammar, Y. A.; Zaki, Y. H. Convenient Synthesis of Some New Thiophene, Pyrazole, and Thiazole Derivatives Bearing Biologically Active Sulfonyl Guanidine Moiety. Polycycl. Aromat. Compd. 2021, 1–19.
[46] Abdelhamid, A. O.; El Sayed, I. E.; Zaki, Y. H.; Hussein, A. M.; Mangoud, M. M.; Hosny, M. A. Utility of 5-(Furan-2-yl)-3-(p-Tolyl)-4,5-Dihydro-1H-Pyrazole-1-Carbothioamide in the Synthesis of Heterocyclic Compounds with Antimicrobial Activity. BMC Chem. 2019, 13(1), 1–18.
[47] Gomha, S. M.; Zaki, Y. H.; Abdelhamid, A. O. Utility of 3-Acetyl-6-Bromo-2H-Chromen-2-One for the Synthesis of New Heterocycles as Potential Antiproliferative Agents. Molecules 2015, 20(12), 21826–21839.
[48] Abdelhamid, A. O.; Abdelall, E. K. A.; Zaki, Y. H. Reactions with Hydrazonoyl Halides 62: Synthesis and Antimicrobial Evaluation of Imidazo[1,2-a]Pyrimidine, Imidazo[1,2-a]Pyridine, Imdazo[1,2-b]Pyrazole, and Quinoxaline Derivatives. J. Heterocycl. Chem. 2010, 47(2), 477–482.
[49] El-Naggar, M.; Gomha, S. M.; Abd El-Ghany, N. A.; Abolibda, T. Z.; Alruwaili, A. H.; Zaki, M. E. A.; Ebaid, M. S.; Mohamed, N. A. Green Synthesis and Molecular Docking Studies of Bisthiazole and Bisthiadiazole Derivatives Using p-Aminobenzoic Acid Chitosan/CuONP Composites. Green Chem. Lett. Rev. 2025, 18(1), 2511197.
[50] Ait Elmachkouri, Y.; Irrou, E.; Ouachtak, H.; Zaki, M. E. A.; Gomha, S. M.; Oubella, A.; Alotaibi, S. H.; Labd Taha, M. In Silico Studies of Pyrazolopyranopyrimidine as a Potential Anticancer Inhibitor: Synthesis, Network Pharmacology, ADMET Prediction. J. Mol. Struct. 2025, 1343, 142829.
[51] Badrey, M. G.; Zaki, M. E. A.; Farag, B.; Gomha, S. M. Synthesis of Bis-Pyrimidothiazine and Bis-Pyrimidothiadiazinone Derivatives as VEGFR2/KDR Inhibitors via Michael and Mannich Reactions. J. Mol. Struct. 2025, 1344, 142968.
[52] Gomha, S. M.; Muhammad, Z. A.; Gaber, H. M.; Amin, M. M. Synthesis of Some Novel Heterocycles Bearing Thiadiazoles as Potent Anti-Inflammatory and Analgesic Agents. J. Heterocycl. Chem. 2017, 54, 2708–2716.
[53] Rashdan, H. R. M.; Abdelmonsef, A. H.; Shehadi, I. A.; Gomha, S. M.; Soliman, A. M.; Mahmoud, H. K. Synthesis, Molecular Docking Screening and Anti-Proliferative Potency Evaluation of Some New Imidazo[2,1-b]thiazole-Linked Thiadiazole Conjugates. Molecules 2020, 25, 4997.
[54] Alghamdi, A.; Abouzied, A. S.; Alamri, A.; Anwar, S.; Ansari, M.; Khadra, I.; Zaki, Y. H.; Gomha, S. M. Synthesis, Molecular Docking, and Dynamic Simulation Targeting Main Protease (Mpro) of New Thiazole-Clubbed Pyridine Scaffolds as Potential COVID-19 Inhibitors. Curr. Issues Mol. Biol. 2023, 45(2), 1422–1442.
[55] Abbas, I. M.; Abdallah, M. A.; Gomha, S. M.; Kazem, M. S. H. Synthesis and Antimicrobial Activity of Novel Azolopyrimidines and Pyrido-Triazolo-Pyrimidinones Incorporating Pyrazole Moiety. J. Heterocycl. Chem. 2017, 54(6), 3447–3457.
[56] Gomha, S. M.; Abdel-Aziz, H. A. Enaminones as Building Blocks in Heterocyclic Preparations: Synthesis of Novel Pyrazoles, Pyrazolo[3,4-d]pyridazines, Pyrazolo[1,5-a]pyrimidines, Pyrido[2,3-d]pyrimidines Linked to Imidazo[2,1-b]thiazole System. Heterocycles 2012, 85(9), 2291–2303.
[57] Alqarni, S.; Zaki, M. E. A.; Alruwaili, A. H.; El-Naggar, M.; Alafnan, A.; Almansour, K.; Huwaimel, B.; Abouzied, A. S.; Gomha, S. M. Design, Synthesis, Antimicrobial Evaluation, and In Silico Insights of Novel Thiazole-Based Benzylidene Thiazolidinones as Gyrase Inhibitors. J. Biochem. Mol. Toxicol. 2025, 39, e70367.

[58] Ouf, S. A.; Gomha, S. M.; Farag, B.; Zaki, M. E.; Ewies, M. M.; Sharawy, I. A.; Khalil, F. O.; Mahmoud, H. K. Synthesis of Novel Bis-1,2,4-Triazolo[3,4-b][1,3,4]Thiadiazines from Natural Camphoric Acid as Potential Anti-Candidal Agents. Results Chem. 2024, 7, 101406.
[59] Lin, E.-S.; Huang, Y.-H.; Yang, P.-C.; Peng, W.-F.; Huang, C.-Y. Complexed Crystal Structure of the Dihydroorotase Domain of Human CAD Protein with the Anticancer Drug 5-Fluorouracil. Biomolecules 2023, 13(1), 149.
[60] Labute, P. J. Protonate3D: Assignment of Ionization States and Hydrogen Coordinates to Macromolecular Structures. Proteins: Struct., Funct., Bioinform. 2009, 75(1), 187–205.
[61] Yuan, S.; Chan, H. S.; Hu, Z. Using PyMOL as a Platform for Computational Drug Design. Wiley Interdiscip. Rev.: Comput. Mol. Sci. 2017, 7(2), e1298.
[62] DeLano, W. L. PyMOL: An Open-Source Molecular Graphics Tool. CCP4 Newsl. Protein Crystallogr. 2002, 40(1), 82–92.
[63] Gomha, S. M.; Abolibda, T. Z.; Alruwaili, A. H.; Farag, B.; Boraie, W. E.; Al-Hussain, S. A.; Zaki, M. E.; Hussein, A. M. Efficient Green Synthesis of Hydrazide Derivatives Using L-Proline: Structural Characterization, Anticancer Activity, and Molecular Docking Studies. Catalysts 2024, 14(8), 489.
[64] Pires, D. E.; Blundell, T. L.; Ascher, D. B. pkCSM: Predicting Small-Molecule Pharmacokinetic and Toxicity Properties Using Graph-Based Signatures. J. Med. Chem. 2015, 58(9), 4066–4072.
[65] [68] Cao, D.; Wang, J.; Zhou, R.; Li, Y.; Yu, H.; Hou, T. ADMET Evaluation in Drug Discovery. Pharmacol. Kinetics Knowledge Base (PKKB): A Comprehensive Database of Pharmacokinetic and Toxic Properties for Drugs. J. Chem. Inf. Model. 2012, 52(5), 1132–1137.
[66] Cumming, J. G.; Davis, A. M.; Muresan, S.; Haeberlein, M.; Chen, H. Chemical Predictive Modelling to Improve Compound Quality. Nat. Rev. Drug Discov. 2013, 12(12), 948–962.
[67] Gomha, S. M.; Abbas, I. M.; Elaasser, M. M.; Mabrouk, B. K. A. Synthesis, Molecular Docking and Pharmacological Study of Pyrimido-Thiadiazinones and Its Bis-Derivatives. Lett. Drug Des. Discov. 2017, 14, 434–443.
[68] Gomha, S. M.; Riyadh, S. M.; Alharbi, R. A.; Zaki, M. E.; Abolibda, T. Z.; Farag, B. Green Route Synthesis and Molecular Docking of Azines Using Cellulose Sulfuric Acid under Microwave Irradiation. Crystals 2023, 13(2), 260.
[69] Mooers, B. H. Shortcuts for Faster Image Creation in PyMOL. Protein Sci. 2020, 29(1), 268–276.
[70] Lill, M. A.; Danielson, M. L. Computer-Aided Drug Design Platform Using PyMOL. J. Comput.-Aided Mol. Des. 2011, 25, 13–19.